UC Berkeley
UC Berkeley Previously Published Works

Title
Influence of Pore Size on Carbon Dioxide Diffusion in Two Isoreticular Metal–Organic Frameworks

Permalink

Authors
Forse, Alexander C
Colwell, Kristen A
Gonzalez, Miguel I
et al.

Peer reviewed

Influence of Pore Size on Carbon Dioxide Diffusion in Two Isoreticular Metal–Organic Frameworks

Alexander C. Forse,[1,2,3,*] Kristen A. Colwell,[2] Miguel I. Gonzalez,[1] Stefan Benders,[4] Rodolfo M. Torres-Gavosto,[1] Bernhard Blümich,[4] Jeffrey A. Reimer,[2,5,*] Jeffrey R. Long[1,2,5,*]

[1]Department of Chemistry and [2]Department of Chemical and Biomolecular Engineering, University of California Berkeley, Berkeley, California 94720, United States.

[3]Department of Chemistry, University of Cambridge, Cambridge, CB2 1EW, U.K.

[4]Institut für Technische und Makromolekulare Chemie (ITMC), RWTH Aachen University, Worringerweg 2, D-52074 Aachen, Germany.

[5]Materials Sciences Division, Lawrence Berkeley National Laboratory, Berkeley, California 94720, United States

ABSTRACT: The rapid diffusion of molecules in porous materials is critical for numerous applications including separations, energy storage, sensing, and catalysis. A common strategy for tuning guest diffusion rates is to vary the material pore size, although detailed studies that isolate the effect of changing this particular variable are lacking. Here, we begin to address this challenge by measuring the diffusion of carbon dioxide in two isoreticular metal–organic frameworks featuring channels with different diameters, $Zn_2(dobdc)$ ($dobdc^{4-}$ = 2,5-dioxidobenzene-1,4-dicarboxylate) and $Zn_2(dobpdc)$ ($dobpdc^{4-}$ = 4,4′-dioxidobiphenyl-3,3′-dicarboxylate), using pulsed field gradient NMR spectroscopy. An increase in the pore diameter from 15 Å in $Zn_2(dobdc)$ to 22 Å in $Zn_2(dobpdc)$ is accompanied by an increase in the self-diffusion of CO_2 by a factor of 4 to 6, depending on the gas pressure. Analysis of the diffusion anisotropy in $Zn_2(dobdc)$ reveals that the self-diffusion coefficient for motion of CO_2 along the framework channels is at least 10,000 times greater than for motion between the framework channels. Our findings should aid the design of improved porous materials for a range of applications where diffusion plays a critical role in determining performance.

INTRODUCTION

The diffusion of molecules in porous materials underpins numerous technologies, including electrochemical energy storage,[1] catalysis,[2,3] and molecular separations.[4] In the context of separations, diffusion can limit the rate at which adsorption–desorption cycles can be performed in adsorption-based processes and it directly influences the selectivity for different products in membrane separations. Regardless of the application, pore size plays a critical role in determining diffusion in porous materials. Early studies of a series of carbon-based molecular sieves showed that the self-diffusion of water and ethanol increases as a function of pore size,[5] and more recent work on electrolyte ion diffusion in porous carbon electrodes has shown similar effects.[1,6] These carbon materials have highly disordered structures, however, and it is very challenging to probe the effect of pore size while keeping all other structural features constant.

This difficulty has motivated the use of crystalline metal–organic frameworks (MOFs) as model systems for diffusion studies, as these microporous materials have well-defined and tunable pore geometries.[7–10] Some frameworks can be prepared with different pore sizes by expansion of the parent organic linkers

to form families of materials with the same framework topology (known as isoreticular MOFs),[11,12] making them excellent model systems for diffusion studies. For example, $Zn_2(dobdc)$ ($dobdc^{4-}$ = 2,5-dioxidobenzene-1,4-dicarboxylate) and $Zn_2(dobpdc)$ ($dobpdc^{4-}$ = 4,4′-dioxidobiphenyl-3,3′-dicarboxylate) have very similar crystal structures, but their different linker lengths give rise to pore diameters of approximately 15 and 22 Å, respectively (Figure 1). Importantly, these materials, along with their diamine-functionalized variants, have been shown to be promising candidates for CO_2 capture.[13–19] Many ^{13}C NMR studies have established the utility of [13]CO_2 as a probe of molecular motion in MOFs,[20–27] and we have previously studied diffusion of adsorbed [13]CO_2 in $Zn_2(dobpdc)$ using pulsed field gradient (PFG) NMR spectroscopy.[29] Here, we extend this work to explore the diffusion of adsorbed [13]CO_2 in both $Zn_2(dobdc)$ and $Zn_2(dobpdc)$ to examine the influence of pore size on this diffusion. We find that a relatively small increase in the pore diameter can have significant impacts on CO_2 diffusion, and we quantify the very large diffusion anisotropies in $Zn_2(dobdc)$ and $Zn_2(dobpdc)$.

RESULTS AND DISSCUSSION
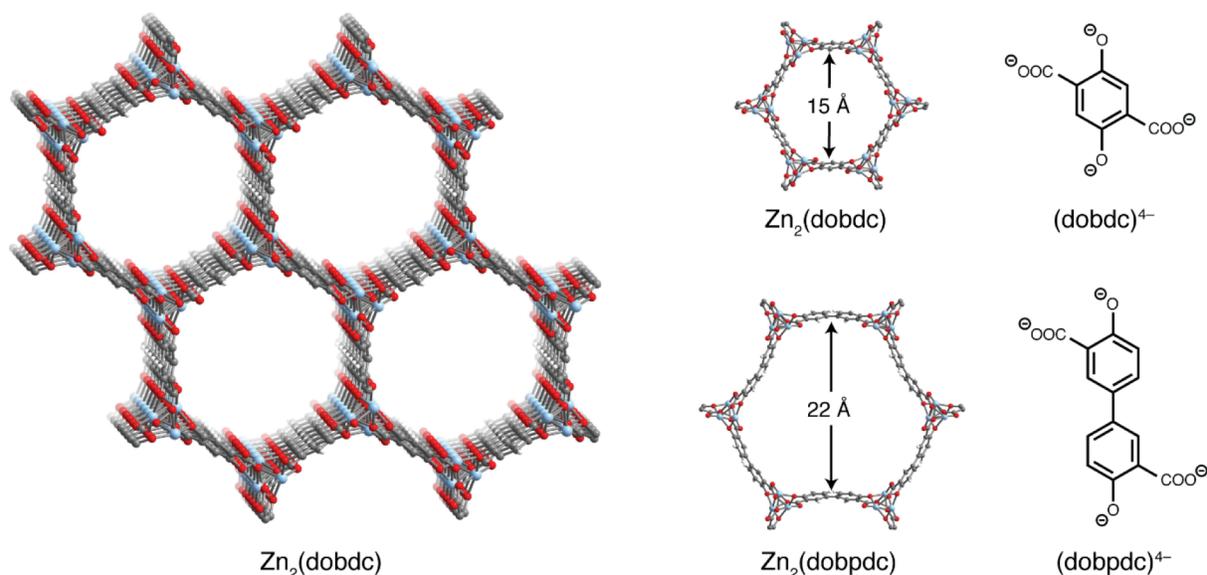
Figure 1. Two Metal–Organic Frameworks with Different Pore Sizes. Left, a portion of the crystal structure of $Zn_2(dobdc)$. Right, views of a single pore of $Zn_2(dobdc)$ and $Zn_2(dobpdc)$ alongside illustrations of their respective ligands. Pale blue, grey, red, and white spheres represent Zn, C, O, and H atoms, respectively.

The metal–organic frameworks $Zn_2(dobdc)$ and $Zn_2(dobpdc)$ were synthesized as large crystals (Figure S1) suitable for single-crystal x-ray diffraction studies and measurement of intracrystalline diffusion via PFG NMR spectroscopy. Diffraction studies of CO_2 adsorption in both materials at 298 K confirmed that the open Zn^{2+} coordination sites exposed upon activation of the materials provide the primary binding site for CO_2, in agreement with previous work (Figure S2).[28] At a lower temperature of 100 K, it was also possible to resolve a secondary binding site in $Zn_2(dobdc)$ where CO_2 is adsorbed adjacent to the primary site (see crystallographic information files). At 298 K, the $M–O_{CO_2}$ distances are 2.44(3) and 2.528(12) Å in $Zn_2(dobdc)$ and $Zn_2(dobpdc)$, respectively, suggesting slightly weaker adsorption of CO_2 in the larger-pore material, an observation that is further supported by CO_2 adsorption isotherm data (Figure S3).

Carbon-13 NMR spectra collected for $Zn_2(dobdc)$ samples dosed with varying pressures of $^{13}CO_2$ show residual chemical shift anisotropy lineshapes (Figures 2 and S4), with the magnitude of the residual anisotropy depending on the CO_2 pressure, as observed previously for $Mg_2(dobdc)$ and $Mg_2(dobpdc)$ variants.[20-22] Importantly, the spectral contributions of CO_2 molecules occupying crystals with different orientations relative to the applied magnetic field (Figure 2a) appear at different NMR frequencies, providing the opportunity to study anisotropic diffusion,[25,26,29,30] *i.e.*, the self-diffusion coefficients parallel to ($D_{//}$) and perpendicular to ($D_\perp$) the one-dimensional channels running along the *c* axes within the MOF crystal structures (Figure 2b).

PFG NMR spectra were first collected for $Zn_2(dobdc)$ dosed with 492 mbar of $^{13}CO_2$ with the magnetic field gradients applied along the *z*-direction. These data revealed that CO_2 diffusion in $Zn_2(dobdc)$ is highly anisotropic (Figure 2c), with the signal intensities decaying at vastly different rates, depending on the chemical shift (*i.e.*, depending on the crystallite orientation). Applying our recently developed analysis method,[30] we extracted a self-diffusion coefficient of $D_{//} = 1.5(4) \times 10^{-9}$ m²s⁻¹ for diffusion along the MOF channels (Figures 2d and S5). The value for $D_{//}$ is comparable to the self-diffusion coefficient of liquid water under ambient conditions[31] $(2.3 \times 10^{-9}$ m²s⁻¹$)$ and smaller than the diffusion of free CO_2 gas[32] $(D = 1.1 \times 10^{-5}$ m²s⁻¹ at 25 °C and 1 bar) by four orders of magnitude.

From our PFG NMR experiments, we were unable to definitively determine whether $D_\perp$ is zero or non-zero (Figure S6), and based on our analysis we estimate an upper limit for $D_\perp$ of 10^{-13} m²s⁻¹, at least eight orders of magnitude smaller than the diffusion of free CO_2.[31] Using these values of $D_{//}$ and $D_\perp$, we obtained simulated NMR spectra that show good agreement with the experimental spectra (Figures 2d and S6). From the results of our PFG NMR experiments, we also calculate a root mean square displacement of 10 μm along the MOF channels, which is much smaller than the typical crystal sizes of on the order of 100 μm employed in the experiments (Figure S1). Thus, exchange with the gas phase is expected to be minimal on the timescale of the measurement. Experiments carried out with $^{13}CO_2$ pressures of 282 and 3578 mbar gave very similar results to the experiments at 492 mbar (Figures S5, and S8–S10), with $D_{//} = 1.0(3) \times 10^{-9}$ and $1.4(4) \times 10^{-9}$ m²s⁻¹, respectively (Figure 3); for both pressures we again estimated $D_\perp < 1 \times 10^{-13}$ m²s⁻¹. Finally, PFG NMR experiments and simulations carried out with the magnetic field gradient applied in the laboratory *x*-direction also yielded consistent values for $D_{//}$ and $D_\perp$ (Figure S7).
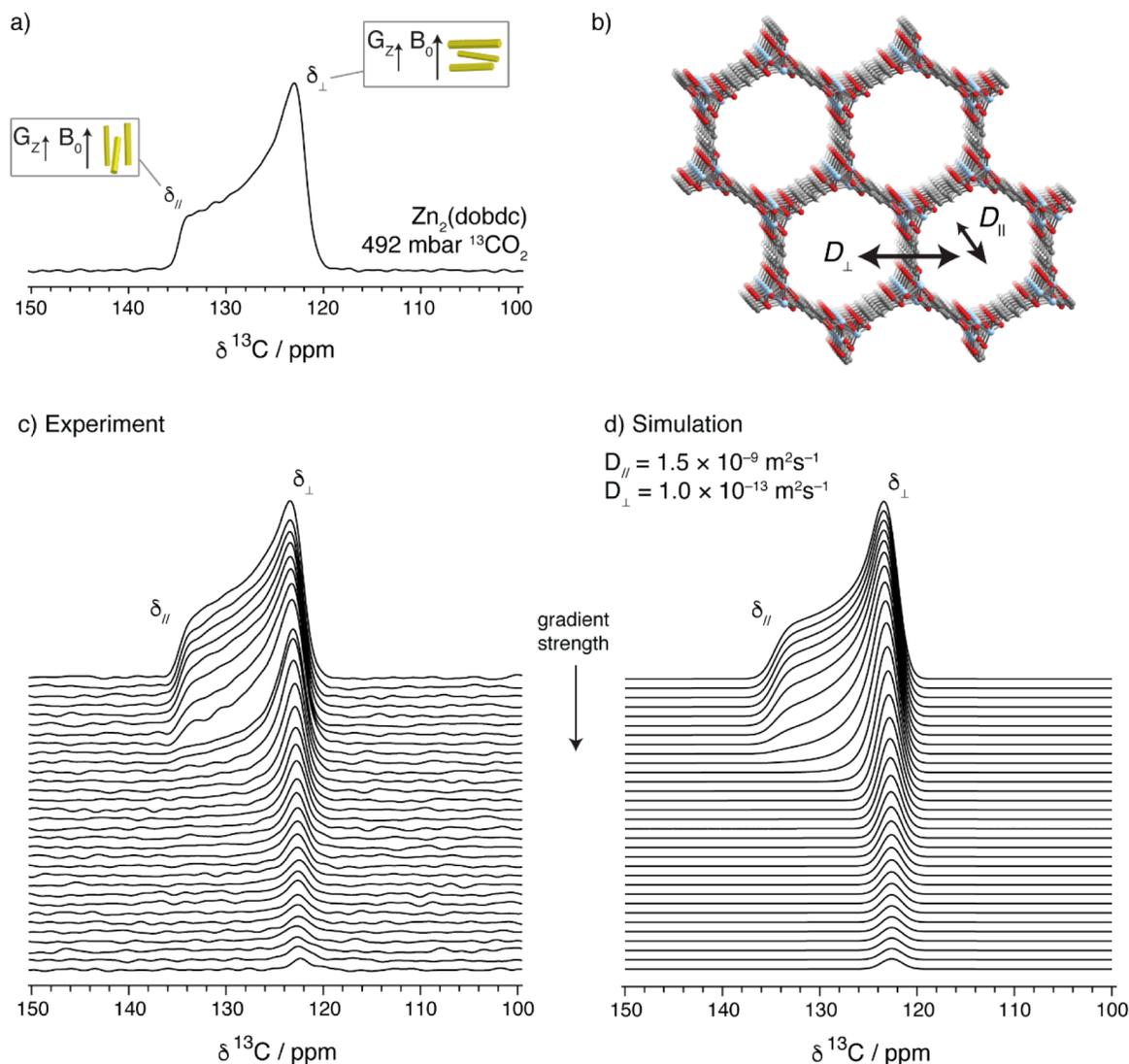
Figure 2. Highly Anisotropic CO_2 Diffusion in $Zn_2(dobdc)$. a) Static quantitative ^{13}C NMR (7.1 T, 25 °C) spectrum of $Zn_2(dobdc)$ dosed with 492 mbar $^{13}CO_2$. b) A portion of the crystal structure of $Zn_2(dobdc)$ showing how $D_{//}$ and $D_\perp$ are defined. c) PFG NMR spectra with the applied magnetic field gradient in the z-direction (parameters: Δ = 31.4 ms. δ' = 2 ms, gradient pulse stabilisation time (t_s) = 1 ms, τ = 5.2 ms, maximum g = 18.0 T m^{-1}). d) Simulated PFG NMR spectra with $D_{//}$ = 1.5 × 10^{-9} m²s^{-1}, $D_\perp$ = 1.0 × 10^{-13} m²s^{-1}, $\delta_{//}$ = 134.7 ppm, $\delta_\perp$ = 122.4 ppm; Gaussian peaks with a FWHM of 2.2 ppm were used to model the homogeneous lineshape).

Given the upper bound for $D_\perp$, the ratio $D_{//}/D_\perp$ is at least 10^4, illustrating that CO_2 diffusion in $Zn_2(dobdc)$ is highly anisotropic. This result is consistent with our prior investigation of CO_2 diffusion in $Zn_2(dobpdc)$[29,30] as well as a recent study on proton conductivity in single crystals of $Co_2(dobdc)$, which found that conductivity along the channels was 1200 times greater than the conductivity in the perpendicular direction.[33] Such large transport anisotropies can be well understood by considering the structure of the $M_2(dobdc)$ materials, wherein the walls of the one-dimensional channels are expected to be largely impermeable (Figure 1, left). The substantial diffusion anisotropy may also support a previous hypothesis that pore obstruction (*e.g.*, resulting from unreacted ligand or crystal defects) accounts for the inaccessibility of some adsorption sites in $M_2(dobdc)$ compounds;[28] indeed, negligible cross-pore diffusion combined

with partially occluded channels could render some adsorption sites completely inaccessible on the timescale of adsorption experiments. We note that previous studies of diffusion in materials with nominally one-dimensional pores have generally shown non-zero $D_\perp$, which is usually attributed to the presence of defects that enable diffusion between neighboring one-dimensional channels.[34,35] We note that the very high diffusion anisotropies obtained in the present study are consistent with a high level of crystallinity.

Analogous measurements performed with the larger pore $Zn_2(dobpdc)$ framework under 2078 mbar $^{13}CO_2$ afforded $D_{//}$ = 5.3(1) × 10^{-9} m²s^{-1} (Figures 3, S5, and S11), similar to our previous work.[29,30] We also measured $D_\perp$ < 6 × 10^{-13} m²s^{-1} (Figure S12), which is significantly smaller than the $D_\perp$ values we
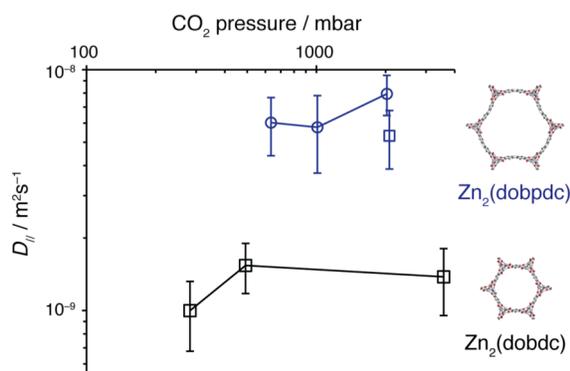
Figure 3. Effect of Pore Diameter upon Diffusion. Self-diffusion coefficients for CO_2 diffusion parallel to the channels within $Zn_2(dobdc)$ and $Zn_2(dobpdc)$. Two data sets are shown for two independent $Zn_2(dobpdc)$ samples, circles are data from our previous work,[29,30] and the data point from this work is shown as a square. Errors represent 95% confidence bounds.

determined in our previous analysis of this material (1.6–4.6×10^{-11} m^{2}s^{-1}).[30] In our previous work, we postulated that structural defects led to diffusion within the *ab*-plane (between the channels) of the framework. The discrepancies between our two studies most likely arise from the different synthesis methods used for $Zn_2(dobpdc)$, which may have led to different defect levels in the two materials. We note that the Langmuir surface area of the $Zn_2(dobpdc)$ sample studied in the present work is greater than that of the material in our previous work (3440 versus 2605 m^2/g),[29] which is consistent with high crystallinity and likely a lower level of defects.

Compared to the value of $D_{//}$ determined for $Zn_2(dobdc)$, $D_{//}$ is consistently greater for $Zn_2(dobpdc)$ by a factor of 4 to 6 (Figure 3). This difference is significant, given the relatively small difference in the pore sizes of these materials (15 versus 22 Å). Previous density functional theory (DFT) calculations of molecular diffusion within $Mg_2(dobdc)$ showed that diffusive pathways down the middle of the channel have considerably lower activation barriers than diffusion between the open metal sites located on the channel walls.[36] We therefore postulate that the presence of additional pore volume in $Zn_2(dobpdc)$ (in the pore center, remote from open metal sites) favors these lower-barrier pathways and accounts for the greater observed self-diffusion. As we noted above, the CO_2–Zn interaction at the primary binding sites also appears to be slightly stronger in $Zn_2(dobdc)$ than in $Zn_2(dobpdc)$, which will also partly account for the lower CO_2 diffusion rate in $Zn_2(dobdc)$. Indeed, previous DFT work also showed that CO_2 hopping between primary binding sites is another important diffusion mode.[36]

We note the Langmuir surface area measured for $Zn_2(dobdc)$ in this work is slightly lower than typical literature values (920 m^2/g versus 1000–1280 m^2/g, respectively),[28,37,38] while our measured Langmuir surface area for $Zn_2(dobpdc)$ compares favorably to literature values (3440 m^2/g versus 2970–3100 m^2/g, respectively).[14,15,39] The lower surface area measured here for $Zn_2(dobdc)$ could indicate either the presence of defects or unwanted molecules (*e.g.*, unreacted ligand) in the pores of our

large crystals, which could then decrease CO_2 self-diffusion and accentuate the differences in diffusion between the two frameworks. We do however expect this effect to be minor, especially given the similar $D_{//}$ values for our two independent $Zn_2(dobpdc)$ samples (Figure 3), which have markedly different Langmuir surface areas (3440 versus 2605 m^2/g). Lastly, we note that there is relatively little variation in $D_{//}$ as a function of pressure from 282–3578 mbar for $Zn_2(dobdc)$ and 635–2078 mbar for $Zn_2(dobpdc)$.[29,30] This is despite significant changes in CO_2 adsorption amounts, e.g. for $Zn_2(dobdc)$ the adsorbed quantity varies from 3.7 to 5.0 to >6.4 mmol/g for CO_2 pressures of 282, 492 and 3578 mbar, respectively (Figure S3). Future experiments with a better signal-to-noise ratio and at more extreme pressures may allow for pressure-dependent diffusion behavior to be observed, as recently reported for methane diffusion in $M_2(dobdc)$ materials.[40]

CONCLUSION

The foregoing results reveal the highly anisotropic nature of self-diffusion of CO_2 in $Zn_2(dobdc)$ and demonstrate that diffusion along the MOF channels ($D_{//}$) is reduced by at least four orders of magnitude compared to free CO_2 gas, with values comparable to that of liquid water diffusion at ambient conditions. We further estimated an upper limit for the diffusion of CO_2 between the channels ($D_\perp$) in $Zn_2(dobdc)$ and found that the self-diffusion coefficient in this perpendicular crystal direction is at least four orders of magnitude smaller than $D_{//}$. By comparing self-diffusion in two isoreticular frameworks with different pore sizes, $Zn_2(dobdc)$ and $Zn_2(dobpdc)$, we have been able quantify the important role of pore size on CO_2 diffusion. In particular, a relatively small change of pore size from 15 to 22 Å leads to increases in the self-diffusion coefficient $D_{//}$ by a factor of 4–6, depending on the CO_2 pressure. Future efforts will focus on expanding this analysis to explore a larger family of isoreticular frameworks with differing pore sizes, such that a quantitative relationship between pore size and diffusion can be determined. Future efforts would also benefit from analysis of diffusion under mixed-gas conditions that are more relevant to real-world applications.[41–43] Insights from studies of this type and related foregoing work will ultimately assist in the design of improved adsorbents and membranes for gas separations.

EXPERIMENTAL SECTION

Synthesis of $Zn_2(dobdc)$. H_4dobdc (500 mg, 2.52 mmol) was dissolved in 250 mL of ethanol. Separately, $Zn(CH_3CO_2)_2 \cdot 2H_2O$ (1950 mg, 8.88 mmol) was dissolved in 250 mL of deionized water. Then, 5-mL aliquots of each solution were combined in a 20-mL scintillation vial. To seal the vial, Teflon tape was first wrapped around the glass thread and the plastic lid was then tightly closed. The vial was further sealed using electrical tape. The vial was placed in a 75 °C oven for approximately 2 h, at which point yellow, needle-shaped crystals had formed. The contents of approximately 20–30 vials prepared in this manner were combined in a glass jar and were washed with deionized water three times, and then six times with methanol. For all washes, the solution above the sedimented crystals was decanted and then replaced with pure solvent (~40 mL), and the resulting crystal/fresh solvent mixture was heated at 60 °C for at least 1 h before the next wash. The crystals were stored in a jar of methanol until they needed to be used for further experiments. For NMR experiments, the crystals were transferred to 8 mm diameter valved-NMR tubes (Norell) while still solvated by methanol, and they were then activated for

39 h at 180 °C under high vacuum using a turbomolecular pump. Activated $Zn_2(dobdc)$ crystals were obtained as yellow needles. A Langmuir surface area of 920 m^2/g was determined from N_2 adsorption isotherm measurements performed at 77 K.

Synthesis of $Zn_2(dobpdc)$. $H_4dobpdc$ (280 mg, 1.03 mmol) was dissolved in 100 mL of ethanol in a Schlenk flask. Separately, $Zn(CH_3CO_2)_2 \cdot 2H_2O$ (780 mg, 3.55 mmol) was dissolved in 100 mL of deionized water in a 500-mL round bottom flask, which had been silanized with chlorotrimethylsilane (2% in toluene). The solutions were both sparged for 1 h with nitrogen gas, at which point the ligand/ethanol solution was cannula-transferred into the 500-mL round bottom flask containing the zinc acetate solution. The combined solution was then heated at 75 °C in an oil bath for 12 h, after which time white needle-shaped crystals had formed. This procedure was performed twice and the crystalline products were combined. The reaction liquid was decanted and was replaced with fresh N,N-dimethylformamide (DMF) and left to stand for 12 h. Next, two 3-h washes were carried out sequentially with each of the following solvents: DMF, MeOH, CH_2Cl_2. Washes were performed at room temperature in a glovebox (95% N_2, 5% H_2). The crystals were then transferred to a valved NMR tube and activated for 63 h at 180 °C under high vacuum using a turbomolecular pump. The $Zn_2(dobpdc)$ crystals were obtained as off-white needles. A Langmuir surface area of 3440 m^2/g was determined from N_2 adsorption isotherm measurements performed at 77 K.

Sample Preparation for NMR Experiments. MOF crystals were transferred to valved NMR tubes, as described above, and were then activated inside the NMR tubes. Note that the as-purchased valved 5 mm NMR tubes were modified to have an outer diameter of 8 mm so they could best fill the 8 mm detection coil used for NMR experiments. Samples were evacuated on a custom gas dosing manifold[29] and then dosed with $^{13}CO_2$ gas (Sigma-Aldrich, 99 atom % ^{13}C, <3 atom % ^{18}O) at ambient temperature, with at least 30 min allowed for equilibration. Finally, the pressure was recorded using a capacitance manometer (MKS instruments, model 722B) and the Teflon valve on the NMR tube was closed before detaching the tube from the manifold and performing NMR experiments.

Pulsed Field Gradient NMR Measurements and Data Analysis. All NMR experiments were performed in static mode with a 7.0 T horizontal magnet and using a Bruker solution-state NMR probe equipped with an 8 mm coil. Diff30 and microimaging attachments were used for experiments with magnetic field gradients applied along the z- and x-directions, respectively. A 90° pulse length of 35 μs for ^{13}C gave a radiofrequency field strength of 7.1 kHz. ^{13}C NMR chemical shifts were referenced to the ethylene carbon of neat ethanol at 57.4 ppm as a secondary reference relative to tetramethylsilane (1 vol % in deuterated chloroform) at 0.0 ppm. Sine-shaped gradient pulses were used in all PFG NMR measurements. Initial calibration of the gradient strength was carried out via stimulated echo ^{1}H PFG NMR experiments performed on water at 25 °C with a known self-diffusion coefficient of 2.3×10^{-9} $m^2 s^{-1}$.[31] Additional PFG NMR experiments were carried out on ethylene glycol and glycerol at 298 K to confirm that the known self-diffusion coefficients[44,45] could be reproduced.

For PFG NMR experiments performed on CO_2-dosed MOF samples, the 13-interval pulse sequence with bipolar magnetic field gradient pulses was used (Figure S13).[46] Sine-shaped gradient pulses were used. The effective durations of the individual magnetic field gradient pulses (δ'), the delays between the RF pulses (τ), the gradient pulse stabilization times (t_s) and diffusion delays (Δ) are given in the figure captions and are defined graphically in Figure S13. Diffusion delays were set to integer multiples of the period (20 ms) of the 50 Hz mains alternating current to mitigate potential issues from residual mains hum.[47]

We define θ as the angle between the long axis of the needle-shaped crystals and the applied magnetic field, B_0, direction. The decay of the NMR signal with the applied gradient applied along the z-direction is then governed by the following equations:

$$\delta = \delta_{//}cos^2\theta + \delta_{\perp}sin^2\theta \qquad [1]$$

$$D_{\text{eff},z} = D_{//}cos^2\theta + D_{\perp}sin^2\theta \qquad [2]$$

$$\frac{I(b)}{I(b_0)} = a \cdot \exp\left(-b \cdot D_{\text{eff},z}\right) \qquad [3]$$

$$b = (2\delta'\gamma g)^2\left(\Delta + \frac{3\tau}{2} - \frac{\delta'}{6}\right) \qquad [4]$$

where equation [1] gives the chemical shift (δ) of CO_2 located in a crystal at angle θ relative to B_0, given residual chemical shift anisotropy parameters $\delta_{//}$ and $\delta_{\perp}$. Equation [2] gives the effective diffusion coefficient for CO_2 in a given crystal obtained from PFG NMR measurements, where the magnetic field gradient is applied along the z-direction ($D_{\text{eff},z}$). Equations [3] and [4] give the signal decay observed in pulsed-field gradient NMR experiments performed with the 13-interval sequence,[46] where $I(b)$ is the integrated signal intensity for a given b value, g is the applied magnet field gradient strength, b_0 is the b value at the smallest g used, and γ is the gyromagnetic ratio of the studied nucleus (see also Figure S13).

Analysis of the PFG NMR data was undertaken in a manner very similar to our previous approach.[30] First, $D_{//}$ values were obtained by fits of the PFG NMR signal intensities integrated over a small range of chemical shifts at $\delta_{//}$. Second, spectral simulations in a Matlab code[30] were carried out to estimate the magnitude $D_{\perp}$. Third, additional experiments that probe larger b values (i.e., experiments with stronger gradients, larger g) were carried out and analyzed to estimate a lower-limit value of $D_{\perp}$. We simulated the NMR response from CO_2 in 28656 crystallites with different orientations (φ, θ), relative to B_0, according to the Zaremba, Conroy, and Wolfsberg scheme for sampling the spherical coordinate space, as implemented in Simpson software.[48] Gaussian peaks with a FWHM of 2.2 ppm were used to model the homogeneous lineshape (i.e., the lineshape from the spectral contribution of CO_2 in a single crystal). Additional details on these simulations are given in our previous work.[30]

X-Ray Diffraction. A methanol-solvated crystal of $Zn_2(dobdc)$ was mounted on a borosilicate glass fiber using a minimal amount of epoxy in air, ensuring that the crystal pores at the two ends of the crystal remained accessible. The glass fiber was then inserted into a 1.0 mm borosilicate glass capillary, which was connected to a HiP Taper Seal valve using a Swagelok Ultra-Torr vacuum fitting with a Viton O-ring. The capillary-dosing assembly was then attached to a port on a Micromeretics ASAP 2420 instrument using a Cajon VCO fitting. The capillary was evacuated under reduced pressure at 180 °C for 24 h to remove solvent molecules that fill the pores and coordinate to the Zn centers within the crystal. The capillary was dosed with 900 mbar of CO_2, and was then flame-sealed using a methane/oxygen torch. Details of diffraction experiments on $Zn_2(dobpdc)$ are provided in our previous work.[29]

X-ray diffraction data were collected at Beamline 12.2.1 at the Advanced Light Source, Lawrence Berkeley National Laboratory using

synchrotron radiation (λ = 0.7288 Å) with a Bruker Photon II CMOS detector. Data were collected at 100 K (for $Zn_2(dobdc)\cdot2.0CO_2$) and 298 K (for $Zn_2(dobdc)\cdot1.0CO_2$), with the sample temperature maintained using an Oxford Cryosystems cryostream.

The crystals of each compound were found to be non-merohedral twins, based on analysis of diffraction patterns. For each structure, CELL_NOW[49] was used to determine the orientation matrices. Raw data for both twin matrices were integrated and corrected for Lorentz and polarization effects using Bruker AXS SAINT software[50] and corrected for absorption using TWINABS.[51] TWINABS was used to produce a merged HKLF4 file for structure solution and initial refinement and an HKLF5 file for final structure refinement. The structures were solved using direct methods with SHELXS[52,53] and refined using SHELXL[54,55] operated in the OLEX2 interface.[56] Thermal parameters were refined anisotropically for all non-hydrogen atoms. Disorder and thermal motion of the bound gas molecules required the use of displacement parameter and distance restraints. All hydrogen atoms were refined using the riding model.

Gas Adsorption Measurements. Gas adsorption measurements were carried out using a Micromeritics ASAP 2420 instrument. Nitrogen adsorption isotherms at 77 K are shown in Figure S3 and were used to determine Langmuir surface areas. Carbon dioxide adsorption isotherms at 21 °C are also shown Figure S3.

ASSOCIATED CONTENT

Supporting Information

The Supporting Information is available free of charge on the ACS Publications website.

Microscope images of crystals, gas adsorption data, additional NMR spectra and simulations, additional crystallographic data (PDF).

Crystallographic data for $Zn_2(dobdc)\cdot(CO_2)_{1.0}$ at 298 K (CIF).

Crystallographic data for $Zn_2(dobdc)\cdot(CO_2)_{2.0}$ at 100 K (CIF).

AUTHOR INFORMATION

Corresponding Author

*acf50@cam.ac.uk (A.C.F.)

*reimer@berkeley.edu (J.A.R.)

*jrlong@berkeley.edu (J.R.L.)

ACKNOWLEDGEMENTS

REFERENCES

(1)   Borchardt, L.; Leistenschneider, D.; Haase, J.; Dvoyashkin, M. Revising the Concept of Pore Hierarchy for Ionic Transport in Carbon Materials for Supercapacitors. *Adv. Energy Mater.* **2018**, *8*, 1–8.

(2)   Gao, W.-Y.; Cardenal, A. D.; Wang, C.-H.; Powers, D. C. In Operando Analysis of Diffusion in Porous Metal-Organic Framework Catalysts. *Chem. Eur. J.* **2018**, 10.1002/chem.201804490.

(3)   Xiao, D. J.; Oktawiec, J.; Milner, P. J.; Long, J. R. Pore Environment Effects on Catalytic Cyclohexane Oxidation in Expanded Fe2(Dobdc) Analogues. *J. Am. Chem. Soc.* **2016**, *138*, 14371–14379.

(4)   Karger, J.; Ruthven, D. M.; Theodorou, D. N. *Diffusion in Nanoporous Materials*; Wiley-VCH, 2012.

(5)   Dubinin, M. M.; Vartapetian, R. S.; Voloshchuk, A. M.; Karger, J.; Pfeifer, H. NMR Study of Translational Mobility of Molecules Adsorbed on Active Carbons. *Carbon N. Y.* **1988**, *26*, 515–520.

(6)   Forse, A. C.; Griffin, J. M.; Merlet, C.; Carretero-Gonzalez, J.; Raji, A.-R. O.; Trease, N. M.; Grey, C. P. Direct Observation of Ion Dynamics in Supercapacitor Electrodes Using in Situ Diffusion NMR Spectroscopy. *Nat. Energy* **2017**, *2*.

(7)   Stallmach, F.; Gröger, S.; Künzel, V.; Kärger, J.; Yaghi, O. M.; Hesse, M.; Müller, U. NMR Studies on the Diffusion of Hydrocarbons on the Metal-Organic Framework Material MOF-5. *Angew. Chem. Int. Ed. Engl.* **2006**, *45*, 2123–2126.

(8)   Eum, K.; Jayachandrababu, K. C.; Rashidi, F.; Zhang, K.; Leisen, J.; Graham, S.; Lively, R. P.; Chance, R. R.; Sholl, D. S.; Jones, C. W.; et al. Highly Tunable Molecular Sieving and Adsorption Properties of Mixed-Linker Zeolitic Imidazolate Frameworks. *J. Am. Chem. Soc.* **2015**, *137*, 4191–4197.

(9)   Berens, S.; Chmelik, C.; Hillman, F.; Jeong, H.; Vasenkov, S. Ethane Diffusion in Mixed Linker Zeolitic Imidazolate Framework-7-8 by Pulsed Field Gradient NMR in Combination with Single Crystal IR Microscopy. *Phys. Chem. Chem. Phys.* **2018**, *20*, 23967–23975.

(10)   Popp, T. M. O.; Plantz, A. Z.; Yaghi, O. M.; Reimer, J. A. Precise Control of Molecular Self-Diffusion in Isoreticular and Multivariate Metal-Organic Frameworks. *Chem. Phys. Chem.* **2019**, *20*.

(11)   Eddaoudi, M.; Kim, J.; Rosi, N.; Vodak, D.; Wachter, J.; O'Keeffe, M.; Yaghi, O. M. Systematic Design of Pore Size and Functionality in Isoreticular MOFs and Their Application in Methane Storage. *Science* **2008**, *295*, 469–472.

(12)   Deng, H.; Grunder, S.; Cordova, K. E.; Valente, C.; Furukawa, H.; Hmadeh, M.; Gándara, F.; Whalley, A. C.; Liu, Z.; Asahina, S.; et al. Large-Pore Apertures in a Series of Metal-Organic Frameworks. *Science* **2012**, *336*, 1018–1024.

(13)   McDonald, T. M.; Mason, J. A.; Kong, X.; Bloch, E. D.; Gygi, D.; Dani, A.; Crocellà, V.; Giordanino, F.; Odoh, S. O.; Drisdell, W. S.; et al. Cooperative Insertion of CO2 in Diamine-Appended Metal-Organic Frameworks. *Nature* **2015**, *519*, 303–308.

(14)   Siegelman, R. L.; McDonald, T. M.; Gonzalez, M. I.; Martell, J. D.; Milner, P. J.; Mason, J. A.; Berger, A. H.; Bhown, A. S.; Long, J. R. Controlling Cooperative CO2 Adsorption in Diamine-Appended Mg2(Dobpdc) Metal–Organic Frameworks. *J. Am. Chem. Soc.* **2017**, *139*, 10526–10538.

(15)   Milner, P. J.; Siegelman, R. L.; Forse, A. C.; Gonzalez, M. I.; Runčevski, T.; Martell, J. D.; Reimer, J. A.; Long, J. R. A Diaminopropane-Appended Metal–Organic Framework Enabling Efficient CO2 Capture from Coal Flue Gas via a Mixed Adsorption Mechanism. *J. Am. Chem. Soc.* **2017**, *139*, 13541–13553.

(16)   Forse, A. C.; Milner, P. J.; Lee, J.-H.; Redfearn, H. N.; Oktawiec, J.; Siegelman, R. L.; Martell, J. D.; Dinakar, B.; Porter-Zasada, L. B.; Gonzalez, M. I.; et al. Elucidating CO2 Chemisorption in Diamine-Appended Metal-Organic Frameworks. *J. Am. Chem. Soc.* **2018**, *140*, 18016–18031.

(17)   Lee, W. R.; Jo, H.; Yang, L.-M.; Lee, H.; Ryu, D. W.; Lim, K. S.; Song, J. H.; Min, D. Y.; Han, S. S.; Seo, J. G.; et al. Exceptional CO 2 Working Capacity in a Heterodiamine-Grafted Metal–Organic Framework. *Chem. Sci.* **2015**, *6*, 3697–3705.

(18)   Jo, H.; Lee, W. R.; Kim, N. W.; Jung, H.; Lim, K. S.; Kim, J. E.; Kang, D. W.; Lee, H.; Hiremath, V.; Seo, J. G.; et al. Fine-Tuning of the Carbon Dioxide Capture Capability of Diamine-Grafted Metal–Organic Framework Adsorbents Through Amine Functionalization. *Chem. Sus. Chem.* **2017**, *2*, 541–550.

(19)   Lee, W. R.; Kim, J. E.; Lee, S. J.; Kang, M.; Kang, D. W.; Lee, H. Y.;

Hiremath, V.; Seo, J. G.; Jun, H.; Moon, D.; et al. Diamine-Functionalization of a Metal – Organic Framework Adsorbent for Superb Carbon Dioxide Adsorption and Desorption Properties. *Chem. Sus. Chem.* **2018**, *11*, 1694–1707.

(20) Lin, L.-C.; Kim, J.; Kong, X.; Scott, E.; McDonald, T. M.; Long, J. R.; Reimer, J. A.; Smit, B. Understanding CO2 Dynamics in Metal-Organic Frameworks with Open Metal Sites. *Angew. Chem. Int. Ed. Engl.* **2013**, *52*, 4410–4413.

(21) Kong, X.; Scott, E.; Ding, W.; Mason, J. A.; Long, J. R.; Reimer, J. A. CO2 Dynamics in a Metal−Organic Framework with Open Metal Sites. *J. Am. Chem. Soc.* **2012**, *134*, 14341–14344.

(22) Marti, R. M.; Howe, J. D.; Morelock, C. R.; Conradi, M. S.; Walton, K. S.; Sholl, D. S.; Hayes, S. E. CO2 Dynamics in Pure and Mixed-Metal MOFs with Open Metal Sites. *J. Phys. Chem. C* **2017**, *121*, 25778–25787.

(23) Zhang, Y.; Lucier, B. E. G.; Huang, Y. Deducing CO2 Motion, Adsorption Locations and Binding Strengths in a Flexible Metal–Organic Framework without Open Metal Sites. *Phys. Chem. Chem. Phys.* **2016**, *18*, 8327–8341.

(24) Schaber, J.; Krause, S.; Paasch, S.; Senkovska, I.; Bon, V.; Többens, D. M.; Wallacher, D.; Kaskel, S.; Brunner, E. In Situ Monitoring of Unique Switching Transitions in the Pressure-Amplifying Flexible Framework Material DUT-49 by High-Pressure Xe NMR Spectroscopy. *J. Phys. Chem. C* **2017**, *121*, 5195–5200.

(25) Peksa, M.; Burrekaew, S.; Schmid, R.; Lang, J.; Stallmach, F. Microporous and Mesoporous Materials Rotational and Translational Dynamics of CO2 Adsorbed in MOF Zn2(Bdc)2(Dabco). *Microporous Mesoporous Mater.* **2015**, *216*, 75–81.

(26) Peksa, M.; Lang, J.; Stallmach, F. 13C NMR Study of Diffusion Anisotropy of Carbon Dioxide Adsorbed in Nanoporous DMOF-1. *Microporous Mesoporous Mater.* **2015**, *205*, 11–15.

(27) Hoffmann, H.; Debowski, M.; Müller, P.; Paasch, S.; Senkovska, I.; Kaskel, S.; Brunner, E. Solid-State NMR Spectroscopy of Metal–Organic Framework Compounds (MOFs). *Materials (Basel).* **2012**, *5*, 2537–2572.

(28) Queen, W. L.; Hudson, M. R.; Bloch, E. D.; Mason, J. A.; Gonzalez, M. I.; Lee, J. S.; Gygi, D.; Howe, J. D.; Lee, K.; Darwish, T. A.; et al. Comprehensive Study of Carbon Dioxide Adsorption in the Metal–Organic Frameworks M 2 (Dobdc) (M = Mg, Mn, Fe, Co, Ni, Cu, Zn). *Chem. Sci.* **2014**, *5*, 4569–4581.

(29) Forse, A. C.; Gonzalez, M. I.; Siegelman, R. L.; Witherspoon, V. J.; Jawahery, S.; Mercado, R.; Milner, P. J.; Martell, J. D.; Smit, B.; Blümich, B.; et al. Unexpected Diffusion Anisotropy of Carbon Dioxide in the Metal−Organic Framework Zn2(Dobpdc). *J. Am. Chem. Soc.* **2018**, *140*, 1663–1673.

(30) Forse, A. C.; Altobelli, S. A.; Benders, S.; Conradi, M. S.; Reimer, A. Revisiting Anisotropic Diffusion of Carbon Dioxide in the Metal−Organic Framework Zn2(Dobpdc). *J. Phys. Chem. C* **2018**, *122*, 15344–15351.

(31) Holz, M.; Heil, S. R.; Sacco, A. Temperature-Dependent Self-Diffusion Coefficients of Water and Six Selected Molecular Liquids for Calibration in Accurate 1 H NMR PFG Measurements. *Phys. Chem. Chem. Phys.* **2000**, *2*, 4720–4742.

(32) Winn, E. B. The Temperature Dependence of the Self-Diffusion Coefficients Of. *Phys. Rev.* **1950**, *80*, 1024–1027.

(33) Hwang, S.; Lee, E. J.; Song, D.; Jeong, N. C. High Proton Mobility with High Directionality in Isolated Channels of MOF-74. *ACS Appl. Mater. Interfaces* **2018**, *10*, 35354–35360.

(34) Stallmach, F.; Karger, J.; Krause, C.; Jeschke, M.; Oberhagemann, U. Evidence of Anisotropic Self-Diffusion of Guest Molecules in Nanoporous Materials of MCM-41 Type. *J. Am. Chem. Soc.* **2000**, *122*, 9237–9242.

(35) Kondrashova, D.; Lauerer, A.; Mehlhorn, D.; Jobic, H.; Feldhoff, A.; Thommes, M.; Chakraborty, D.; Gommes, C.; Zecevic, J.; De Jongh, P.; et al. Scale-Dependent Diffusion Anisotropy in Nanoporous Silicon. *Sci. Rep.* **2017**, *7*, 40207.

(36) Canepa, P.; Nijem, N.; Chabal, Y. J.; Thonhauser, T. Diffusion of Small Molecules in Metal Organic Framework Materials. *Phys. Rev. Lett.* **2013**, *110*, 026102.

(37) Tranchemontagne, D. J.; Hunt, J. R.; Yaghi, O. M. Room Temperature Synthesis of Metal-Organic Frameworks : MOF-5 , MOF-74 ,. *Tetrahedron* **2008**, *64*, 8553–8557.

(38) Yu, D.; Yazaydin, A. O.; Lane, J. R.; Dietzel, P. D. C.; Snurr, R. Q. A Combined Experimental and Quantum Chemical Study of CO2 Adsorption in the Metal–Organic Framework CPO-27 with Different Metals. *Chem. Sci.* **2013**, *4*, 3544–3556.

(39) Gygi, D.; Bloch, E. D.; Mason, J. A.; Hudson, M. R.; Gonzalez, M. I.; Siegelman, R. L.; Darwish, T. A.; Queen, W. L.; Brown, C. M.; Long, J. R. Hydrogen Storage in the Expanded Pore Metal–Organic Frameworks. *Chem. Mater.* **2016**, *28*, 1128–1138.

(40) Witherspoon, V. J.; Mercado, R.; Braun, E.; Mace, A.; Bachman, J.; Long, J. R.; Blumich, B.; Smit, B.; Reimer, J. A. Combined Nuclear Magnetic Resonance and Molecular Dynamics Study of Methane Adsorption in M2(Dobdc) Metal−Organic Frameworks. *J. Phys. Chem. C* **2019**, *123*, 12286–12295.

(41) Tan, K.; Jensen, S.; Zuluaga, S.; Chapman, E. K.; Wang, H.; Rahman, R.; Cure, J.; Kim, T.-H.; Li, J.; Thonhauser, T.; et al. Role of Hydrogen Bonding on Transport of Coadsorbed Gases in Metal−Organic Frameworks Materials. *J. Am. Chem. Soc.* **2018**, *140*, 856–859.

(42) Bendt, S.; Dong, Y.; Keil, F. J. Diffusion of Water and Carbon Dioxide and Mixtures Thereof in Mg-MOF-74. *J. Phys. Chem. C* **2018**, *123*, 8212–8220.

(43) Sin, M.; Kavoosi, N.; Rauche, M.; Pallmann, J.; Paasch, S.; Senkovska, I.; Kaskel, S.; Brunner, E. In Situ 13C NMR Spectroscopy Study of CO2/CH4 Mixture Adsorption by Metal−Organic Frameworks: Does Flexibility Influence Selectivity? *Langmuir* **2019**, *35*, 3162–3170.

(44) Spees, W. M.; Song, S.-K.; Garbow, J. R.; Neil, J. J.; Ackerman, J. J. H. Use of Ethylene Glycol to Evaluate Gradient Performance in Gradient-Intensive Diffusion MR Sequences. *Magn. Reson. Med.* **2012**, *68*, 319–324.

(45) Burnett, L. J.; Harmon, J. F. Self-Diffusion in Viscous Liquids : Pulse NMR Measurements Self-Diffusion in Viscous Liquids : Pulse NMR Measurements. *J. Chem. Phys.* **1972**, *57*, 1293–1297.

(46) Cotts, R. M.; Hoch, M. J. R.; Sun, T.; Markert, J. T. Pulsed Field Gradient Stimulated Echo Methods for Improved NMR Diffusion Measurements in Heterogeneous Systems. *J. Magn. Reson.* **1989**, *266*, 252–266.

(47) Callaghan, P. T. *Principles of Nuclear Magnetic Resonance Microscopy*; Oxford, 1991.

(48) Bak, M.; Rasmussen, J. T.; Nielsen, N. C. SIMPSON : A General Simulation Program for Solid-State NMR Spectroscopy. *J. Magn. Reson.* **2000**, *147*, 296–330.

(49) Sheldrick, G. M. CELL NOW V2008/2. *Bruker AXS Inc* **2008**.

(50) Bruker Analytical X-ray Systems Inc.: Madison, WI, U. SAINT, APEX2, and APEX3 Software for CCD Diffractometers, 2014.

(51) Sheldrick, G. M. TWINABS, Version 2012/1; *Univ. Göttingen* **2012**.

(52) Sheldrick, G. M. SHELXS. *Univ. Göttingen* **2014**.

(53) Sheldrick, G. M. A Short History of SHELX. *Acta Crystallogr., A, Found. Crystallogr.* **2008**, *64*, 112–122.

(54) Sheldrick, G. M. Crystal Structure Refinement with SHELXL. *Acta Crystallogr. Sect. C Struct. Chem.* **2015**, *71*, 3–8.

(55) Sheldrick, G. M. SHELXL. *Univ. Göttingen* **2014**.

(56) Dolomanov, O. V.; Bourhis, L. J.; Gildea, R. J.; Howard, J. A. K.; Puschmann, H. OLEX2: A Complete Structure Solution, Refinement and Analysis Program. *J. Appl. Crystallogr.* **2009**, *42*, 339–341.

TOC IMAGE

Pore size effect on intracrystalline CO_2 diffusion

gas phase diffusion
10^{-5} m²s⁻¹

small channels
1.5×10^{-9} m²s⁻¹

large channels
6×10^{-9} m²s⁻¹